In vitro Biological Characterization of a Novel, Synthetic Diaryl Pyrazole Resorcinol Class of Heat Shock Protein 90 Inhibitors

Swee Y. Sharp,[1] Kathy Boxall,[1] Martin Rowlands,[1] Chrisostomos Prodromou,[2] S. Mark Roe,[2] Alison Maloney,[1] Marissa Powers,[1] Paul A. Clarke,[1] Gary Box,[1] Sharon Sanderson,[1] Lisa Patterson,[1] Thomas P. Matthews,[1] Kwai-Ming J. Cheung,[1] Karen Ball,[1] Angela Hayes,[1] Florence Raynaud,[1] Richard Marais,[3] Laurence Pearl,[2] Sue Eccles,[1] Wynne Aherne,[1] Edward McDonald,[1] and Paul Workman[1]

[1]Haddow Laboratories, Cancer Research UK Centre for Cancer Therapeutics, The Institute of Cancer Research, Surrey, United Kingdom; [2]Chester Beatty Laboratories, Section of Structural Biology; and [3]Cancer Research UK Centre for Cell and Molecular Biology, The Institute of Cancer Research, London, United Kingdom

Abstract

The molecular chaperone heat shock protein 90 (HSP90) has emerged as an exciting molecular target. Derivatives of the natural product geldanamycin, such as 17-allylamino-17-demethoxy-geldanamycin (17-AAG), were the first HSP90 ATPase inhibitors to enter clinical trial. Synthetic small-molecule HSP90 inhibitors have potential advantages. Here, we describe the biological properties of the lead compound of a new class of 3,4-diaryl pyrazole resorcinol HSP90 inhibitor (CCT018159), which we identified by high-throughput screening. CCT018159 inhibited human HSP90β with comparable potency to 17-AAG and with similar ATP-competitive kinetics. X-ray crystallographic structures of the NH_2-terminal domain of yeast Hsp90 complexed with CCT018159 or its analogues showed binding properties similar to radicicol. The mean cellular GI_{50} value of CCT018159 across a panel of human cancer cell lines, including melanoma, was 5.3 μmol/L. Unlike 17-AAG, the *in vitro* antitumor activity of the pyrazole resorcinol analogues is independent of NQO1/DT-diaphorase and P-glycoprotein expression. The molecular signature of HSP90 inhibition, comprising increased expression of HSP72 protein and depletion of ERBB2, CDK4, C-RAF, and mutant B-RAF, was shown by Western blotting and quantified by time-resolved fluorescent-Cellisa in human cancer cell lines treated with CCT018159. CCT018159 caused cell cytostasis associated with a G_1 arrest and induced apoptosis. CCT018159 also inhibited key endothelial and tumor cell functions implicated in invasion and angiogenesis. Overall, we have shown that diaryl pyrazole resorcinols exhibited similar cellular properties to 17-AAG with potential advantages (e.g., aqueous solubility, independence from NQO1 and P-glycoprotein). These compounds form the basis for further structure-based optimization to identify more potent inhibitors suitable for clinical development. [Cancer Res 2007;67(5):2206–16]

Introduction

The molecular chaperone heat shock protein 90 (HSP90) regulates the stability, activation, and biological function of numerous oncogenic client proteins, including steroid hormone receptors, kinases (e.g., ERBB2, C-RAF, B-RAF, and CDK4), and other proteins (e.g., mutant p53, hTERT, and HIF1α; ref. 1). The HSP90 chaperone machine is driven by ATP binding and hydrolysis (2). Its activity is regulated by co-chaperones (e.g., HSP72, CDC37, P23, CHIP, and immunophilins) that affect the balance between stabilization and degradation of clients via the ubiquitin-proteasome pathway (3, 4). HSP90 inhibitors are therefore of interest. Therapeutic selectivity for cancer versus normal cells could derive from the stressed conditions associated with malignancy (5), oncogene addiction, and the greater dependence on HSP90 of mutated versus wild-type oncoproteins, as exemplified recently with B-RAF (6, 7). Because HSP90 client proteins are associated with many oncogenic signaling pathways, pharmacologic blockade of HSP90 function should deliver a combinatorial effect on all the hallmark traits of malignancy (8).

The complex natural products geldanamycin and radicicol (Fig. 1) bind at the NH_2-terminal ATP site and inhibit the ATPase activity (9). This targets client proteins for proteasomal degradation (10, 11), most probably via recruitment of ubiquitin ligases like CHIP (3). Geldanamycin exhibited potent antitumor activity against human cancer cells (12), but significant toxicities precluded its clinical development (13). The geldanamycin derivative 17-allylamino-17-demethoxy-geldanamycin (17-AAG; Fig. 1) exhibited a greater therapeutic window (14–16). Several phase I clinical trials of 17-AAG have been completed (17–19). These showed that 17-AAG is well tolerated with satisfactory pharmacokinetic exposures, leading to HSP90 inhibition as shown by the accepted molecular signature (17, 20). Prolonged stable disease was observed in two patients with metastatic malignant melanoma (17), and responses were also observed in breast cancer and multiple myeloma (21, 22).

Despite these promising results, 17-AAG has potential drawbacks, including limited aqueous solubility with resulting formulation issues, low oral bioavailability (23), variable metabolism by the polymorphic enzymes CYP3A4 (24) and NQO1/DT-diaphorase (15, 25), and hepatotoxicity (17–19). 17-DMAG (26) and the hydroquinone IPI-504 (27), which exhibit improved aqueous solubility, have entered phase I clinical trials. Radicicol analogues showed *in vivo* activity in human tumor xenografts (28) but have not progressed to the clinic.

Experience with the natural products generated interest in alternative chemotypes (29–31). The first synthetic small-molecule

Note: Supplementary data for this article are available at Cancer Research Online (http://cancerres.aacrjournals.org/).

Requests for reprints: Paul Workman, Haddow Laboratories, Cancer Research UK Centre for Cancer Therapeutics, The Institute of Cancer Research, 15 Cotswold Road, Belmont, Sutton, Surrey, SM2 5NG, United Kingdom. Phone: 44-208-722-4301; Fax: 44-208-722-4324; E-mail: Paul.Workman@icr.ac.uk.

doi:10.1158/0008-5472.CAN-06-3473

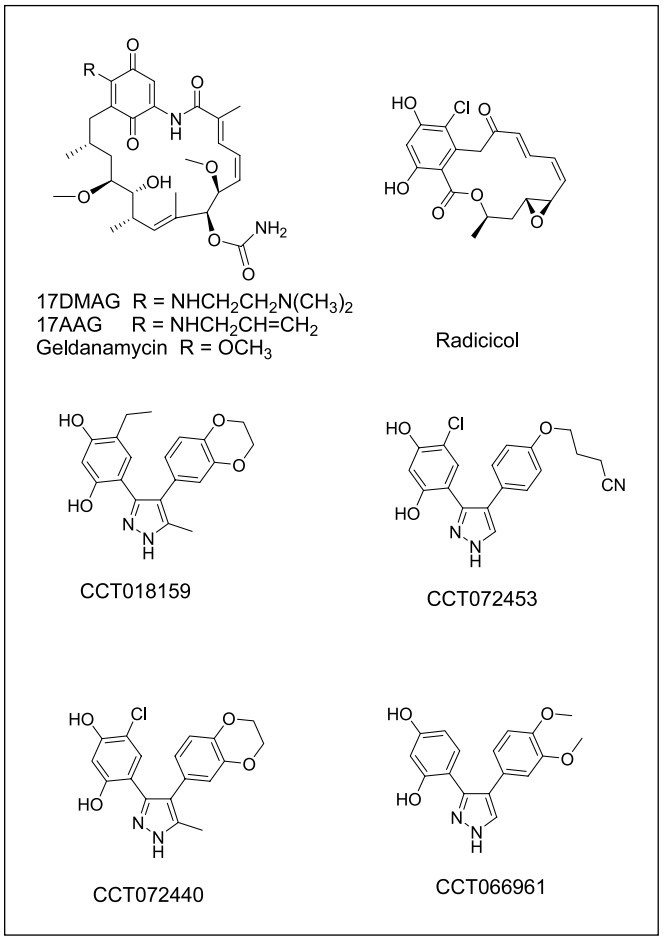

Figure 1. Chemical structures of the different classes of HSP90 inhibitors.

NH_2-terminal ATP site–binding inhibitors were designed by Chiosis et al. based on a purine scaffold (32, 33). Purines with improved aqueous solubility and oral bioavailability have been described (33).

Using high-throughput screening to identify inhibitors of the intrinsic NH_2-terminal ATPase activity of yeast Hsp90 (34), we discovered the novel synthetic 3,4-diaryl pyrazole resorcinol inhibitor CCT018159 (35). Structure-based design generated a series of active analogues (36, 37). Here, we provide the first detailed characterization of the biological properties of CCT018159 and related derivatives. The results show that CCT018159 is a representative of a new class of fully synthetic molecules with potential for development as novel anticancer agents.

Materials and Methods

HSP90 inhibitors. Diaryl pyrazole resorcinols were synthesized as described (35). 17-AAG and radicicol were from Axxora Ltd. (Nottingham, United Kingdom) and Sigma-Aldrich (Poole, Dorset, United Kingdom), respectively. Geldanamycin was supplied by the National Cancer Institute (Rockville, MD). All compounds were dissolved in DMSO.

Cell lines. Unless otherwise stated, all cell lines were from the American Type Culture Collection (LGC Promochem, Middlesex, United Kingdom). All human cancer cell lines were grown in DMEM /10% FCS, 2 mmol/L glutamine, and nonessential amino acids in 5% CO_2. The human umbilical vein endothelial cells (HUVEC) and the prostate carcinoma cell line PC3LN3 were cultured as described (38). MCF10a cells derived from human mammary gland were maintained in DMEM-Ham's F12 mix (Invitrogen Ltd., Paisley, United Kingdom) and 10% FCS, 10 μg/mL insulin, 20 ng/mL epidermal growth factor, 100 ng/mL cholera toxin, and 500 ng/mL hydrocortisone. The human prostate epithelial cell line PNT2, immortalized with SV40 (European Collection of Animal Cell Cultures, Wiltshire, United Kingdom), was grown in RPMI 1640 (Invitrogen) and 10% FCS. All lines were free of *Mycoplasma* contamination (Venor GeM kit, Minerva Biolabs, Berlin, Germany).

Production of recombinant HSP90 and AHA1. Expression and purification of recombinant full-length human HSP90β, full-length yeast Hsp90, and NH_2-terminal domain and yeast AHA1 was as described (39, 40).

X-ray crystallography. Crystallization of the yeast Hsp90 NH_2-terminal domain has been described (39). An aliquot (5 μL) of inhibitor at 50 mmol/L stock concentration was added to 1 mL of HSP90 NH_2-terminal domain at 4 mg/mL in 20 mmol/L Tris (pH 7.5) and 1 mmol/L EDTA. The complex was concentrated to 200 μL (20 mg/mL) and crystallized by the hanging drop method.

Isothermal titration calorimetry and K_d determinations. Heats of interaction were measured as described (9). Briefly, 10 aliquots of 27 μL compound (100 μmol/L) were injected into 10 μmol/L recombinant full-length human HSP90β at 30°C in 20 mmol/L Tris (pH 7.5), 1 mmol/L EDTA, 5 mmol/L NaCl, and 1% DMSO.

Colorimetric determination of ATPase activity. Inhibition of ATPase activity of recombinant yeast Hsp90 or recombinant human HSP90β in the presence of the co-chaperone AHA1 (40) was determined using the malachite green assay (34). Briefly, different inhibitor concentrations were added to 400 μmol/L ATP (Sigma-Aldrich), 400 nmol/L yeast Hsp90 or 2 μmol/L human HSP90β and 30 μmol/L AHA1 in 100 mmol/L Tris-HCl (pH 7.4), 20 mmol/L KCl, and 6 mmol/L $MgCl_2$. IC_{50} values were determined as the concentration causing 50% inhibition compared with vehicle controls.

K_i values against recombinant full-length human HSP90 ATPase activity were determined as follows. Enzyme activity for 3.3 μg protein was assayed at 2.5 μmol/L compound across a range of ATP concentrations (0.2–2 mmol/L). The double reciprocal plot of 1/velocity against 1/substrate concentration was used to determine the type of inhibition and a secondary plot of x intercept against concentration generated K_i values (Graphpad Prism, San Diego, CA).

Biochemical selectivity of CCT018159. The malachite green assay (34) was used to determine the biochemical selectivity of CCT018159 versus human HSP72 ATPase activity (SPP-776F; Stressgen, Victoria, Canada) at 400 μmol/L ATP and 1.2 μmol/L protein. Selectivity towards human topoisomerase II ATPase was determined using DNA decatenation to measure functional activity (TopoGen assay kit, Port Orange, FL); 200 ng catenated DNA with 6 units of enzyme were used. Kinase profiling was carried out by Upstate (Charlottesville, VA).

Fluorescence polarization assay. Competitive binding of inhibitors to full-length human HSP90β was measured using a fluorescent pyrazole resorcinol probe (41). Relative binding affinities for HSP90 in lysates from cancer and nontumorigenic cell lines were also measured by fluorescence polarization assay.

Growth inhibition assay. Cellular sensitivity to HSP90 inhibitors was measured by sulforhodamine B (SRB) assay (15). Sensitivity of HUVEC was determined using an alkaline phosphatase colorimetric method (38). The GI_{50} was calculated as the concentration that inhibits cell proliferation by 50% compared with vehicle controls.

Western blotting. Protein extracts and Western blotting were done as described (15). Antibodies are described in Supplementary Materials.

Time-resolved fluorescence-Cellisa. Full details of time-resolved fluorescent (TRF)-Cellisa have been described (42).

Cell cycle analysis. Cell cycle effects were initially determined using propidium iodide (PI) staining and flow cytometry (16). For more detailed analysis, bromodeoxyuridine (BrdUrd)-Hoechst33258/PI staining was used.

Apoptosis studies. Attached and trypan blue–negative detached cells were counted using a hemacytometer. Poly(ADP-ribose) polymerase (PARP) cleavage was detected by Western blotting using an antibody (Clontech, Oxford, United Kingdom) that recognizes the 116-kDa native PARP and the 85-kDa apoptosis-related cleavage product (16).

Functional studies on human endothelial and tumor cells. *In vitro* chemomigration in response to soluble ligands, haptotaxis assays (migration on a solid substrate), and cellular differentiation on Matrigel using HUVEC and/or PC3LN3 human prostate carcinoma cells and LICR-LON-HN6 head and neck squamous carcinoma cells were determined as described (38, 43).

Results

Protein X-ray crystallography. Protein X-ray crystallography at 1.6 to 2.5Å resolution confirmed that radicicol, CCT018159, CCT072453, and CCT072440 (Fig. 1) all bind to the ATP site within the yeast Hsp90 NH_2-terminal domain (Fig. 2). The carboxylate side chain of Asp^{79} forms two hydrogen bonds (Fig. 2*A, left*), one via a tightly bound water molecule, to two of the radicicol oxygens (9). The same tightly bound water is hydrogen bonded to the main-chain amide group of Gly^{83} and the hydroxyl side chain of Thr^{171}. Another hydrogen bond exists between the main-chain carbonyl of Leu^{34}, via a second water molecule, to a third radicicol oxygen, and yet another contact is formed between the ε-amino side chain of Lys^{44} and the radicicol epoxide oxygen. Other interactions are van der Waals contacts (Asn^{37}, Asp^{40}, Ala^{41}, Ile^{82}, Met^{84}, Phe^{124}, and Ile^{173}; Fig. 2*A, left*). The pyrazole resorcinol CCT018159 binds similarly (35), except that the hydrophilic Lys^{44} and hydrophobic Asp^{40} interactions are lost (Fig. 2*A, right*). However, an additional hydrophobic interaction is established with Leu^{93}, whereas the main-chain carbonyl of Gly^{83} and one of the ring nitrogens of CCT018159 form a new hydrophobic contact, as with the other pyrazole analogues (Fig. 2*B*). For CCT072453, the protein interactions are exactly the same as for radicicol and include contacts with Lys^{44} and Asp^{40} (Fig. 2*B, left*), but not with Leu^{93} as seen for CCT018159. In contrast, for CCT072440, the Lys^{44} and Asp^{40} interactions are lost, and there is also no interaction with Leu^{93} (Fig. 2*B, right*). The 5′-ethyl group on the resorcinol ring of CCT018159 and the equivalent 5′-chloro group of CCT072440 and CCT072453 reside in a hydrophobic pocket, contributing to potency (see later). The superimpositions (Fig. 2*C*) show that the pyrazole resorcinols and radicicol all occupy a similar space within the HSP90 ATP-binding site.

HSP90 binding and ATPase inhibition. Isothermal titration calorimetry with full-length recombinant human HSP90β gave a dissociation constant (K_d) of 0.47 μmol/L for CCT018159. K_d values were about 2-fold lower for the 5′-chloro analogue CCT072440 (0.24 μmol/L), the 5′-chloro analogue with a cyanopropyloxy substituent replacing the dioxan ring CCT072453 (0.25 μmol/L), and geldanamycin (0.24 μmol/L). The less-potent analogue CCT066961 (Fig. 1), lacking a chloro or ethyl substituent at C-5 in the resorcinol ring, gave a K_d value of 4.0 μmol/L. Radicicol showed tighter binding with a K_d of 0.007 μmol/L. In the presence of recombinant human HSP90 ATPase-activating protein AHA1 (40), CCT018159 binding to HSP90β was similar (K_d = 0.37 μmol/L). Incubation of CCT018159 and geldanamycin for 24 h at room temperature did not markedly alter the K_d (0.53 and 0.32 μmol/L, respectively).

CCT018159, 17-AAG, and geldanamycin acted as competitive inhibitors with respect to ATP against the full-length recombinant human HSP90 ATPase, assayed with AHA1 using the malachite green method. CCT018159 exhibited a K_i of 1.8 ± 0.29 μmol/L (mean ± SE, n = 3), which was similar to that for 17-AAG (1.4 ± 0.32 μmol/L) and geldanamycin (1.8 ± 0.22 μmol/L).

The IC_{50} value for CCT018159 against the ATPase activity of full-length yeast Hsp90 at 400 μmol/L ATP was 6.6 ± 0.5 μmol/L (mean ± SE, n = 3). The 5′-chloro analogues CCT072440 and CCT072453 were 10-fold more potent than CCT018159 (Table 1A). They were also more potent than CCT018159 against the recombinant full-length HSP90β with AHA1, but the difference was smaller (Table 1A). The analogue CCT066961, lacking a chloro or ethyl substituent at C-5 in the resorcinol ring (Fig. 1), was 15-fold less potent against both yeast and human HSP90 compared with CCT018159 (Table 1A).

The more sensitive fluorescence polarization assay gave IC_{50} values for human HSP90β 5- to 10-fold lower than the malachite green method. CCT072440 and CCT072453 were confirmed as 2- to 3-fold more potent than CCT018159, whereas CCT066961 was 12-fold less potent (Table 1A).

The fluorescence polarization assay was used to determine the relative binding affinity of CCT018159, 17-AAG, and geldanamycin for HSP90 in lysates from human tumor cells (HCT116 colorectal and WM266.4 melanoma) and nontumorigenic cells (HUVECs, MCF10a human mammary gland epithelial cells, and PNT2 human prostate epithelial cells). For all three inhibitors, the binding affinity was similar in lysates from tumor and nontumorigenic cells (Table 1B). In each case, the IC_{50} for binding to HSP90 in the cell lysates was about 2-fold lower than that seen with purified recombinant HSP90β.

Biochemical selectivity of CCT018159. At 10 and 100 μmol/L CCT018159, no inhibition was observed against human HSP72

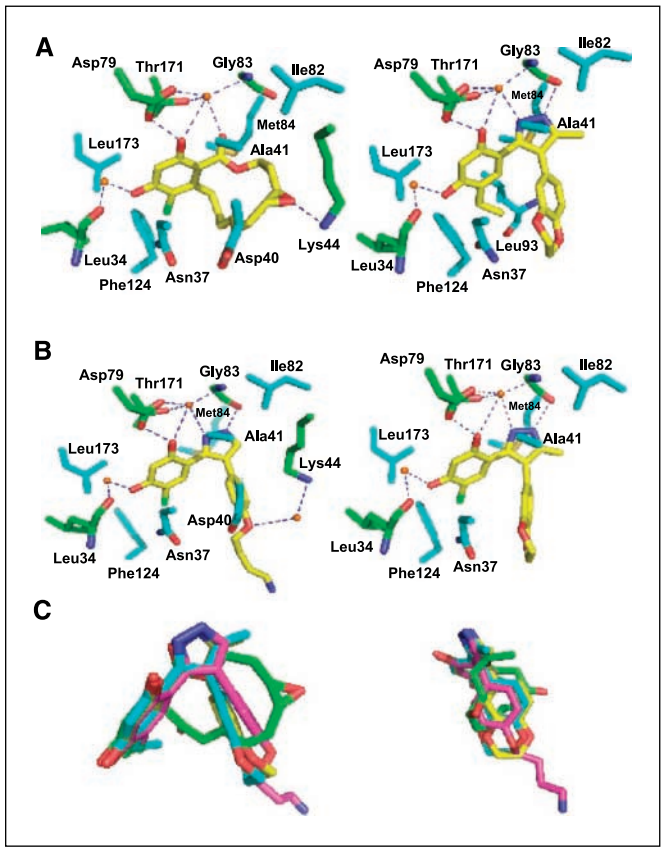

Figure 2. Pymol diagrams obtained from X-ray co-crystal structures showing binding interactions of (*A*) radicicol (*left*) and CCT018159 (*right*) and (*B*) CCT072453 (*left*) and CCT072440 (*right*). Hydrogen bonds (*dotted blue lines*); amino acid residues involved (*green*), water molecules (*orange spheres*), and residues in van der Waals contact (*cyan*). *C, left,* superimposition of radicicol (*green*), CCT018159 (*cyan*), CCT072453 (*pink*) and CCT072440 (*yellow*); *right,* superimposition but with a 90-degree rotation.

Table 1.

A. HSP90 inhibitory and binding activities of CCT018159 and analogues

Compound	IC_{50}, yeast HSP90 ATPase (μmol/L)	IC_{50}, human HSP90β ATPase (μmol/L)	IC_{50}, human HSP90β FP (μmol/L)	GI_{50}, SRB HCT116 cells (μmol/L)
CCT018159	6.6 ± 0.5	3.2 ± 1.5	0.60 ± 0.10	4.1 ± 0.4
CCT072440	0.8 ± 0.2	2.2 ± 0.2	0.20 ± 0.08	4.0 ± 0.6
CCT072453	0.6 ± 0.1	1.8 ± 0.2	0.30 ± 0.02	6.8 ± 0.7
CCT066961	>100	53.0 ± 5.0	7.20 ± 0.30	28.0 ± 1.0

B. Relative binding affinity of HSP90 inhibitors to HSP90 in lysates from human cancer (HCT116 and WM266.4) and nontumorigenic cells (HUVEC, MCF10a, and PNT2) as measured by the fluorescence polarization competitive binding assay using a diaryl pyrazole fluorescent probe (41)

Compound	IC_{50} for binding to HSP90β in human cell lysates (μmol/L)				
	HCT116	WM266.4	HUVEC	MCF10a	PNT2
CCT018159	0.21 ± 0.07	0.22 ± 0.01	0.37 ± 0.04	0.38 ± 0.10	0.16 ± 0.02
17-AAG	0.35 ± 0.13	0.31 ± 0.07	0.35 ± 0.05	0.44 ± 0.09	0.27 ± 0.04
Geldanamycin	0.12 ± 0.03	0.09 ± 0.01	0.09 ± 0.02	0.14 ± 0.02	0.17 ± 0.05

NOTE: (A) Enzyme assays were carried out using full-length yeast Hsp90 or human HSP90β, the latter in the presence of the activating protein AHA1, using the malachite green method (34). The fluorescence polarization competitive binding assay was carried out with human HSP90β using a fluorescent pyrazole resorcinol probe (41). Cell growth inhibitory activities are also shown; these were carried out in HCT116 human colon cancer cells using the SRB endpoint. Values represent mean ± SE (n = 3). (B) The amount of cell lysate that gave an anisotropy reading corresponding to 30 nmol/L human HSP90β was used (4 nmol/L for HCT116 and PNT2 cells and 12 nmol/L for WM266.4, HUVEC, and MCF10a cells). Values represent mean ± SE (n = 3–5).

ATPase or the decatenation activity of human topoisomerase II. In a panel of 20 representative kinases, CCT018159 at 50 μmol/L showed <50% inhibition in 13 of these kinases (Supplementary Table S1). The greatest activity was against LCK (98% inhibition). Note, however, that the concentration used was much higher than the IC_{50} for HSP90β (Table 1).

Antiproliferative activity. The growth-inhibitory potencies of CCT018159, CCT072440, and CCT072453 in HCT116 human colon carcinoma cells, measured by SRB assay, were similar (GI_{50} = 4.1–6.8 μmol/L; Table 1A). CCT066961 was less active, consistent with its lower potency against HSP90β.

The growth-inhibitory activity of CCT018159 was determined against a range of human cancer cell lines. Although CCT018159 was less potent than 17-AAG, in some lines (e.g., CH1 ovarian and BE colon carcinoma), the difference was only 3.6- to 10-fold (Table 2). The mean GI_{50} (±SE) for CCT018159 across the tumor cell panel was 5.3 ± 2.5 μmol/L, with the lowest GI_{50} seen in the MCF7 breast cancer cells (1.4 ± 0.05 μmol/L) and CH1 cells (2.6 ± 0.4 μmol/L). Except for the more resistant HT29 colon carcinoma cell line, the GI_{50} values for CCT018159 varied only 6-fold from 1.4 μmol/L in MCF7 cells to 8.2 μmol/L in SKMEL 5 melanoma cells. In contrast, 17-AAG exhibited a 82-fold range across the cancer cell panel, probably due to varying levels of NQO1 (see later). CCT018159 undergoes rapid glucuronidation both in mice and mouse liver microsomes (44). We showed extensive loss of parent CCT018159 and formation of the corresponding glucuronide in HT29 cells, to a much greater extent than in HCT116 cells (Supplementary Fig. S1), suggesting an explanation for the resistance of HT29 cells.

CCT018159 inhibited HUVEC proliferation with a GI_{50} of 0.87 ± 0.3 μmol/L (mean ± SE, n = 3; Table 2). This indicates greater sensitivity than the tumor cells and is consistent with inhibitory effects of CCT018159 on the functions of activated endothelial cells described later. In contrast, nonmalignant prostate cells (PC3LN3) exhibited similar sensitivity to CCT018159 when compared with majority of the tumor cells tested, whereas mammary epithelial cells (MCF10a) were more resistant. For 17-AAG, HUVEC response was similar to, but not greater than, that of the more sensitive cancer cells. The nontumorigenic breast and prostate epithelial cell lines had GI_{50} values close to those for the more resistant tumor cell lines.

Effect of NQO1/DT-diaphorase on cellular sensitivity to HSP90 inhibitors. We previously reported that cancer cells with low NQO1 levels were much less sensitive to 17-AAG and proposed that this is due to reduction of the quinone to a more active HSP90 inhibitor (15). Recent studies confirmed that the greater activity of 17-AAG in high NQO1 cell lines was caused by metabolism to the more potent hydroquinone (25). Hence, we investigated the effect of NQO1 expression on sensitivity to CCT018159, which lacks the quinone moiety (Fig. 1). The melanoma cell lines exhibit a range of NQO1 activities (15), with SKMEL 5 and WM266.4 expressing the highest levels, SKMEL 28 expressing intermediate level, and SKMEL 2 expressing the lowest activity. This reflects the order of sensitivity to 17-AAG (Table 2). Cellular sensitivity of CCT018159 in the melanoma cell lines did not correlate with NQO1 status. As before (15), 17-AAG was much less active in the BE human colon tumor cells, which carry an inactivating NQO1 polymorphism, compared with HT29 counterparts with naturally high NQO1 levels (P <

Table 2. Sensitivity of human cancer and nontumorigenic cell lines to HSP90 inhibitors

Cell type	Cell line	GI_{50} (μmol/L)	
		CCT018159	17-AAG
Colon carcinoma	HCT116	4.1 ± 0.4	0.016 ± 0.001
	BEneg (vector control)	3.3 ± 0.2	0.340 ± 0.020
	BE2*	3.3 ± 0.4	0.030 ± 0.001
	HT29	23 ± 1.2	0.030 ± 0.010
	HT29oxaliR †	20 ± 1.6	0.040 ± 0.020
Melanoma	SKMEL 2	8.1 ± 1.8	0.059 ± 0.020
	SKMEL 5	8.2 ± 2.7	0.014 ± 0.002
	SKMEL 28	2.9 ± 1.8	0.021 ± 0.005
	WM266.4	6.0 ± 0.1	0.012 ± 0.008
Glioblastoma	SF268	5.1 ± 1.1	0.040 ± 0.011
	U87MG	9.8 ± 0.7	0.028 ± 0.004
Rhabdomyosarcoma	RMS	3.9 ± 0.6	0.020 ± 0.003
Prostate carcinoma	DU145	3.6 ± 0.3	0.012 ± 0.001
Breast carcinoma	MCF7	1.4 ± 0.05	0.009 ± 0.004
Ovarian carcinoma	CH1	2.7 ± 0.5	0.740 ± 0.300
	CH1doxR ‡	3.1 ± 0.1	3.400 ± 0.200
Endothelial cells	HUVEC	0.87 ± 0.30	0.020 ± 0.003
Breast epithelium	MCF10a	5.00 ± 0.005	0.164 ± 0.009
Prostate epithelium	PNT2	19.10 ± 2.25	0.098 ± 0.013

NOTE: Values represent mean ± SE (n = 3–5).
*Transfected with the *NQO1* gene for DT-diaphorase (58).
† Acquired resistance to oxaliplatin (45).
‡ Acquired resistance to doxorubicin, high levels of P-glycoprotein (59).

0.0001; Table 2). Furthermore, 17-AAG was confirmed as less active (P < 0.0001; Table 2) in the BE vector control line compared with its isogenic counterpart transfected with the *NQO1* gene and expressing similar high NQO1 activity to HT29 cells (15). In contrast, CCT018159 showed no differences in potency between this isogenic pair (P = 0.9; Table 2). The GI_{50} values for the 5′-chloro analogue CCT072453 in the BE vector control and transfected BE2 cell lines were also similar (11.0 ± 2.1 and 11.9 ± 1.3 μmol/L, respectively; mean ± SE, n = 3; P = 0.2). These results indicate that unlike 17-AAG, the activity of the pyrazole resorcinols is independent of NQO1.

Sensitivity of acquired drug-resistant cancer cells to HSP90 inhibitors. We previously reported that P-glycoprotein, the product of the *MDR1* multidrug resistance gene, confers resistance to 17-AAG (15). We confirmed that 17-AAG was 4.6-fold less active (P < 0.0001) in the doxorubicin-induced, drug-resistant variant CH1doxR compared with the parental CH1 human ovarian cancer cell line. In contrast, CCT018159 showed no difference in activity between the two lines (P = 0.1; Table 2). The 5′-chloro analogues CCT072453 and CCT072440 also exhibited no cross-resistance (GI_{50} for CCT072453 = 6.8 ± 2.4 μmol/L in the parental CH1 cells and 4.0 ± 1.2 μmol/L in CH1doxR; GI_{50} for CCT072440 = 2.5 ± 0.8 and 2.9 ± 1.1 μmol/L in CH1 and CH1doxR, respectively; P > 0.1). The MDR1 reversal agent R-verapamil reduced the level of doxorubicin resistance to 17-AAG in the CH1doxR from 4.6- to 1.3-fold (GI_{50} values for 17-AAG plus 6 μmol/L R-verapamil in CH1 and CH1doxR were 0.8 ± 0.02 and 1.0 ± 0.01 μmol/L, respectively). No R-verapamil–induced changes in GI_{50} values were observed with CCT018159 (P > 0.1; data not shown). These results suggest that the pyrazole resorcinols are not subject to P-glycoprotein–mediated multidrug resistance.

The *in vitro* potencies of CCT018159 and 17-AAG were also compared in the HT29 human colon cancer cell line and its counterpart with acquired resistance to oxaliplatin (45). CCT018159 and 17-AAG exhibited similar cellular activity in the HT29oxaliR cells compared with the parental line (P = 0.14 and 0.9 for CCT018159 and 17-AAG, respectively; Table 2). Thus, both HSP90 inhibitors are able to retain activity in these platinum-resistant cells.

Molecular signature of HSP90 inhibition induced by CCT018159. 17-AAG causes depletion of client proteins, such as C-RAF, ERBB2, and CDK4, and induction of HSP72 in human cancer cell lines (14–16). This molecular signature of HSP90 inhibition was validated in human tumor xenografts and used to confirm the mechanism of action of 17-AAG in patients (17, 20). Both CCT018159 and 17-AAG induced HSP72 and decreased C-RAF, ERBB2, and CDK4 expression in SKMEL 28 melanoma cells (Fig. 3*A*). A similar level of HSP72 induction and depletion of client proteins by CCT018159 or 17-AAG was also seen in other human cancer cells (e.g., A2780 and CH1 ovarian cells and HT29 and HCT116 colon cells; data not shown except for A2780; Supplementary Fig. S2). The detailed kinetics of client protein depletion was cell line dependent. For example, CCT018159 depleted C-RAF more rapidly in the A2780 line compared with SKMEL 28 (Supplementary Fig. S2; Fig. 3*A*). However, ERBB2 was consistently the most sensitive client protein, as measured by both rapid disappearance (Fig. 3*A*) and by concentration-response data (i.e., depletion at 1 × GI_{50}; data not shown). The 5′-chloro analogues CCT072440 and CCT072453 also showed the same HSP90 inhibition signature in HCT116 cells (data not shown). The less active analogue CCT066961 exhibited no HSP72 induction or client protein depletion at 28 μmol/L (equivalent to

5 × GI_{50} CCT018159; Fig. 3*B*). TRF-Cellisa showed a 2- to 3-fold increase in HSP72 protein levels and 20% to 25% reduction in C-RAF with CCT018159 and CCT072440 in HCT116 cells (Supplementary Fig. S3).

We and others (6, 7) recently reported that oncogenic mutant B-RAF is an HSP90 client protein and is degraded following 17-AAG treatment of melanoma cells. Figure 3*C* shows that CCT018159 and 17-AAG caused comparable depletion of ^{V600E}B-RAF in SKMEL 28 melanoma cells (46). In contrast, no depletion of wild-type B-RAF was seen in SKMEL 5 cells with CCT018159 (Fig. 3*C*) or 17-AAG (6).

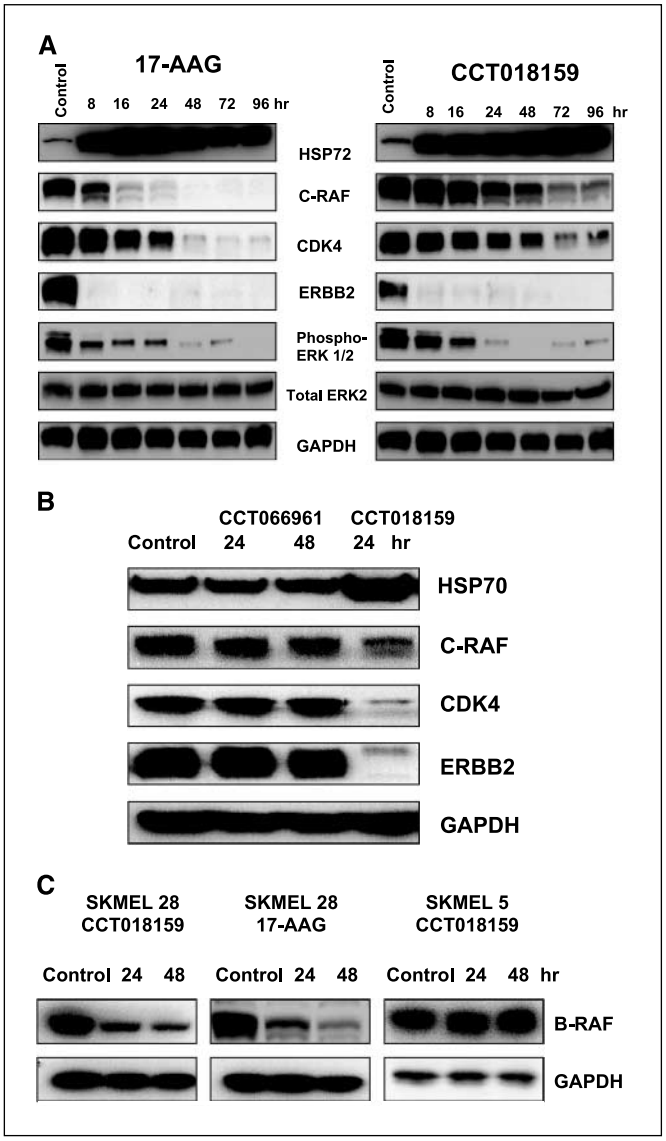

Figure 3. Effects of CCT018159 and 17-AAG on HSP72 induction and client protein depletion. *A,* Western blot of SKMEL 28 cells treated with 5 × GI_{50} concentrations of CCT018159 (14.5 μmol/L) or 17-AAG (0.105 μmol/L) or vehicle control over 96 h. *B,* Western blot of HCT116 human colon cells treated with the less potent compound (CCT066961) at 28 μmol/L, which is equivalent to 5 × GI_{50} of CCT018159 for 24 and 48 h. *C,* Western blot of B-RAF expression after treatment with HSP90 inhibitors in SKMEL 28 (^{V600E}B-RAF mutation) and SKMEL 5 (wild-type B-RAF) melanoma cells. The concentrations of the inhibitors used were 14.5 μmol/L CCT018159 (5 × GI_{50}) and 0.105 μmol/L 17-AAG (5 × GI_{50}) in SKMEL 28 cells and 41 μmol/L CCT018159 (5 × GI_{50}) in WM266.4 cells. Glyceraldehyde-3-phosphate dehydrogenase (*GAPDH*) was used as loading control. Representative blots of at least three independent experiments.

Consistent with depletion of C-RAF and mutant B-RAF, CCT018159 reduced extracellular signal-regulated kinase 1/2 (ERK1/2) phosphorylation without affecting total ERK in SKMEL 28 melanoma (Fig. 3*A*) and other cancer cell lines (data not shown).

Cell cycle effects. Flow cytometry with PI staining showed that CCT018159 or 17-AAG at 5 × GI_{50} concentrations (41 and 0.07 μmol/L, respectively) caused marked accumulation in the G_1 phase in SKMEL 5 (Fig. 4*A*) and other melanoma lines (data not shown). Continuous BrdUrd labeling and bivariate Hoechst-PI flow cytometry showed that both HSP90 inhibitors arrested cells in the initial G_1 or subsequent G_1^* phase (Fig. 4*A*).

Cytostatic versus apoptotic effects. All the melanoma cell lines treated with CCT018159 or 17-AAG showed a cytostatic growth inhibitory response up to 96 h (SKMEL 28 cells shown in Fig. 4*B*). Treatment of SKMEL 28 cells for 24 h with 14.5 μmol/L CCT018159 or 0.105 μmol/L 17-AAG (both equivalent to 5 × GI_{50} concentrations) caused an increase (6- and 1.9-fold, respectively) in trypan blue–negative detached cells (Fig. 4*C*). After 48 h, the number of detached cells after treatment with 17-AAG increased by 8.1-fold (data not shown). Cells treated with CCT018159 resulted in an increased in cell debris after 48 h (data not shown). Apoptosis was confirmed by PARP cleavage in detached SKMEL 28 cells treated with CCT018195 or 17-AAG (Fig. 4*D*). Note in Fig. 4*D* that equal amounts of protein were loaded for the detached treated and control cells, and hence, both also showed similar levels of cleaved PARP. In the controls, this represented the background level of cell death. However, the number of apoptotic cells was increased after treatment with CCT018159 or 17-AAG, when compared with control (Fig. 4*C*).

Functional studies in HUVEC and tumor cells. As shown above (Table 2), HUVECs were very sensitive to growth inhibition by CCT018159. A 24-h exposure of HUVEC to CCT018159 gave a dose-dependent increase in HSP72 and decrease in AKT expression (Fig. 5*A*). CCT018159 also inhibited expression of the major angiogenic cytokine receptor (VEGFR-2). CCT018159 induced a dose-dependent inhibition of HUVEC migration in response to FCS, vascular endothelial growth factor (VEGF), and basic fibroblast growth factor (Fig. 5*B*). Ability to close a "wound" made in confluent cell monolayer (haptotaxis) was inhibited by 60% at 5 × GI_{50} concentrations of CCT018159. Reduction of the HSP90 client protein FAK has been shown to delay haptotaxis (38). CCT018159 reduced FAK phosphorylation at $Tyr^{576/577}$ (47), with moderate effects on total FAK (Fig. 5*A*). CCT018159 reduced the tubular differentiation of HUVEC plated on Matrigel over 24 to 48 h (Fig. 5*C*). In the PC3LN3 prostate tumor cell line, haptotaxis was inhibited by 50% at 5 × GI_{50} concentration of CCT018159. In addition, differentiation of PC3LN3 and LICR-LON HN6 head and neck squamous carcinoma tumor cells on Matrigel (which requires engagement with matrix proteins and cell motility) was reduced by 54% and 72%, respectively, at 5 × GI_{50} concentrations of CCT018159.

These results show that, as exemplified by CCT018159, the diaryl pyrazole resorcinols have the potential to inhibit invasion and angiogenesis as part of their combinatorial anticancer effects, as previously shown for 17-AAG (38).

Discussion

The widely studied HSP90 inhibitors, such as 17-AAG, geldanamycin, and radicicol, inhibit the essential ATPase activity of HSP90 by competing at the NH_2-terminal ATP site (9). However, despite

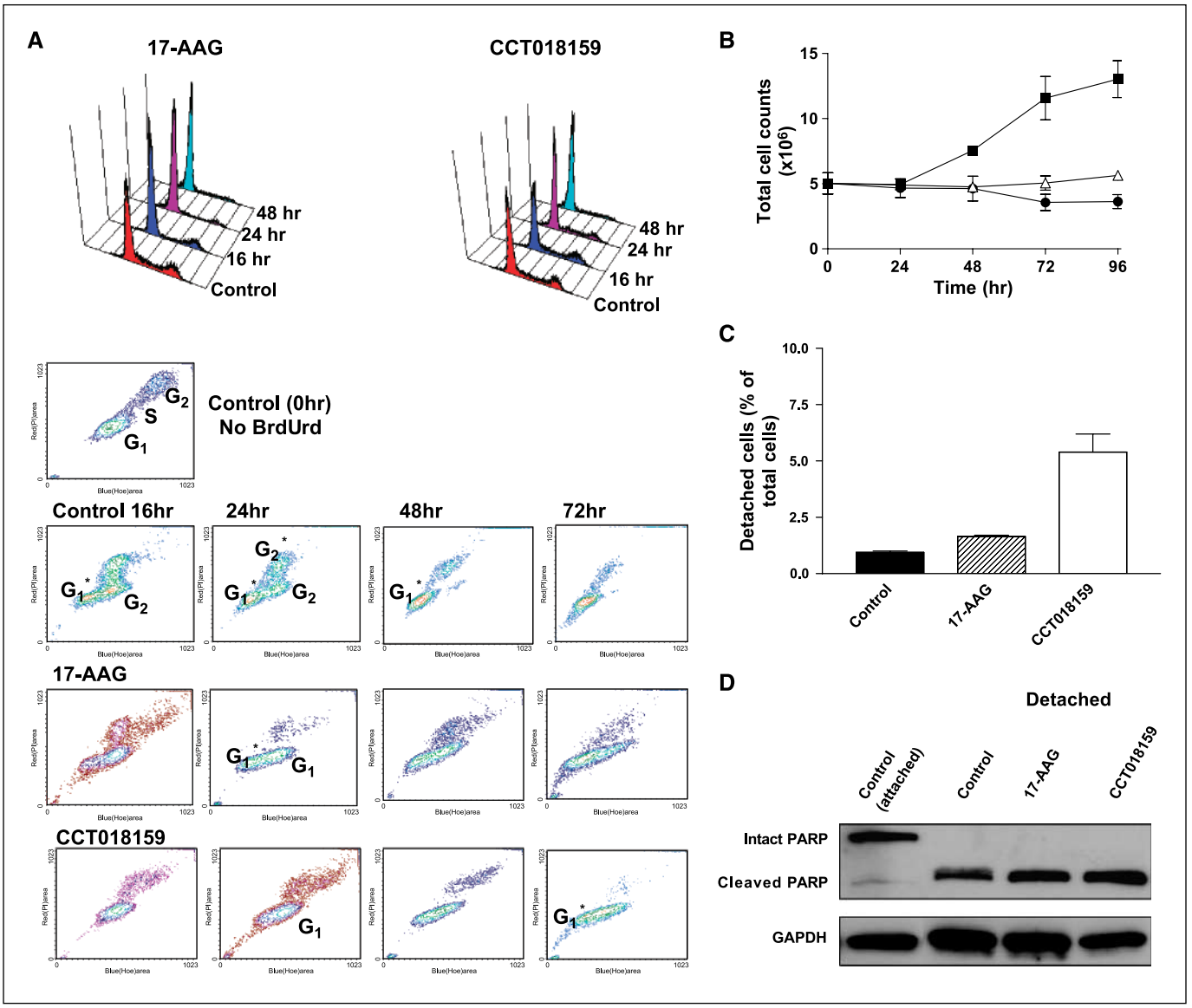

Figure 4. Effects of CCT018159 on cell growth, cell cycle, and apoptosis. *A,* representative DNA histograms and BrdUrd-Hoechst/PI cytograms of SKMEL 5 human melanoma cells following treatment with 41 μmol/L CCT018159 (5 × GI_{50}) or 0.07 μmol/L 17-AAG (5 × IC_{50}). BrdUrd (10 μmol/L) and CCT018159 (or 17-AAG) were added at the same time and incubated for 16, 24, 48, and 72 h before fixing with ethanol. Control cells were treated with vehicle and BrdUrd. No BrdUrd or compound was added to control cells at 0 h. Hoechst/PI stain was added immediately before analysis by flow cytometry. The results were replicated in three independent experiments. Results showed that SKMEL 5 cells treated with CCT018159 or 17-AAG caused a G_1 arrest at 16 h. By 24 h, cells in the original G_2 have moved to the new G_1^* phase and remained blocked at that point. *B,* quantitation of attached total cell counts. SKMEL 28 cells were treated with vehicle control (■) or 14.5 μmol/L CCT018159 (●) or 0.105 μmol/L 17-AAG (△) for 0, 24, 48, 72, and 96 h. Attached cells were counted using a hemacytometer. *C,* detached SKMEL 28 cells (as % total cells) following treatment with 14.5 μmol/L CCT018159, 0.105 μmol/L 17-AAG, or vehicle control for 24 h. *D,* quantitation of detached cells. Equal amounts of protein were loaded from the detached control and treated SKMEL 28 cells after 72 h, and PARP cleavage was detected in both detached populations by Western blotting. The PARP antibody recognizes the 116-kDa native PARP and the 85-kDa apoptosis-related cleavage product. Lysates from the attached population (72 h) were used as control. Note, however, that although PARP cleavage is seen in both control and treated samples, both HSP90 inhibitors caused an increase in the number of detached, apoptotic cells (*C*).

promising molecular effects and clinical activity with 17-AAG (17, 20), the natural product–based inhibitors have significant limitations and synthetic small-molecule inhibitors are eagerly sought (30, 31, 37). The first of these were designed by Chiosis et al. based on the purine scaffold and show considerable promise (32, 33). Next, the diaryl pyrazole resorcinols were identified by high-throughput screening (34, 35, 48). Here, we provide the first detailed description of the biological properties of the lead compound CCT018159 and two related analogues in human cancer cell lines and certain nontumorigenic cells.

Protein X-ray crystallography confirmed that the pyrazole compounds and radicicol, which share the resorcinol unit, bind in a very similar way to the yeast Hsp90 ATP site in the NH_2-terminal domain (Fig. 2*C*). The binding mode involves an intricate network of hydrogen bond interactions between the phenolic hydroxyl groups in the resorcinol moiety of the pyrazoles or radicicol and the protein plus key water molecules. Some specific differences were identified between the pyrazoles and radicicol and between the individual pyrazole compounds. In contrast to radicicol, an additional hydrophilic interaction is established

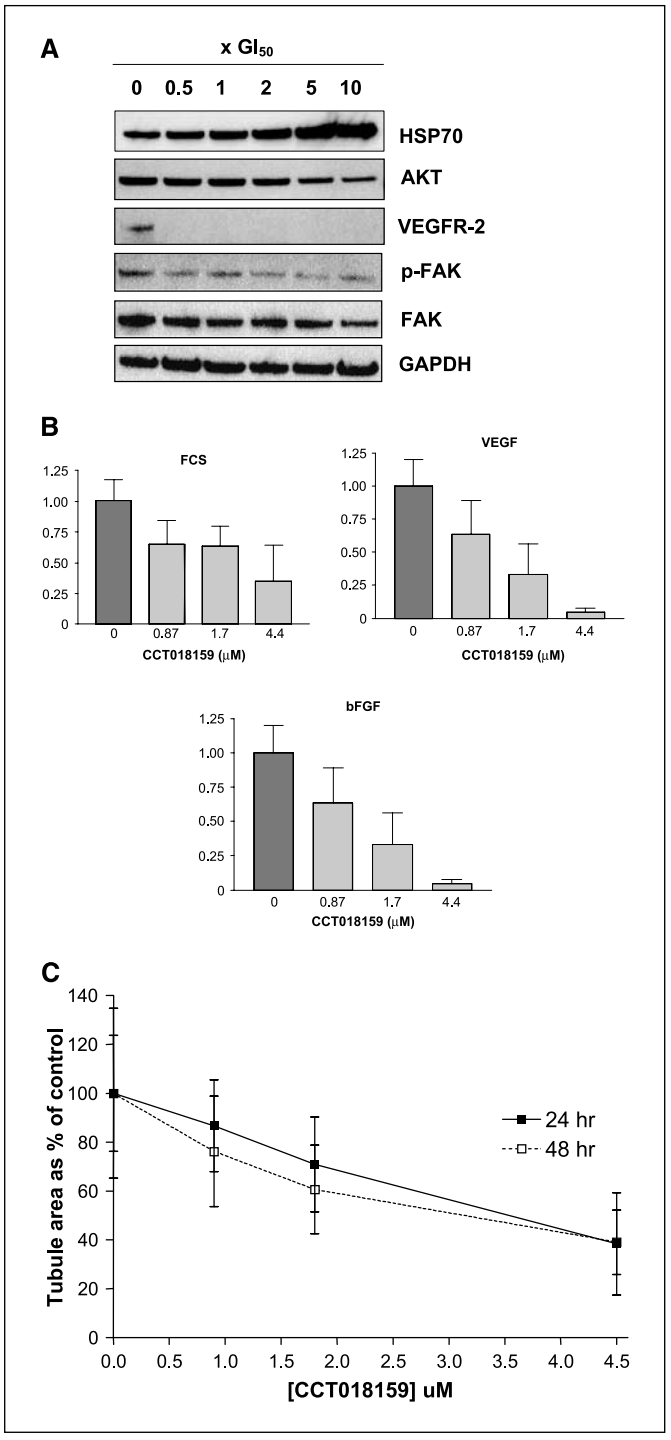

Figure 5. Effects of CCT018159 on various properties of endothelial cells. *A,* Western blot of HUVEC lysates following treatment with multiples of GI_{50} of CCT018159 (1 × GI_{50} = 0.87 μmol/L) for 24 h showing induction of HSP72 and down-regulation of client proteins involved in angiogenesis. *FAK,* focal adhesion kinase. *B,* effects of CCT018159 on cell migration in response to chemokines. HUVECs were treated for 24 h with CCT018159 (at 0.87, 1.7, and 4.4 μmol/L), labeled with CellTracker, and migrated towards 5% FCS for 2 h, 20 ng/mL VEGF for 16 h, or 10 nmol/L bFGF for 16 h. *Columns,* relative number of cells migrating (n = 3); *bars,* SE. *C,* effects of CCT018159 (at 0.87, 1.7, and 4.4 μmol/L) on HUVEC differentiation into pseudocapillaries on Matrigel, which is a surrogate assay of the differentiation/tubulogenesis processes used by endothelial cells during neoangiogenesis. HUVECs were pretreated with CCT018159 for 24 h before seeding onto a layer of Matrigel. Tubule area at 24 and 48 h was quantified using Image Pro-Plus.

between the main-chain carbonyl of Gly^{83} and one of the ring nitrogens of the pyrazoles. The 5′-ethyl group in the resorcinol ring of CCT018159 and the equivalent 5′-chloro group of CCT072440 and CCT072453 occupy a hydrophobic pocket, contributing to potency (see later). The crystallography studies were carried out with yeast Hsp90. The yeast and human enzymes exhibit 88% similarity (70% identity) between their NH_2-terminal domains, with only two differences within 5 Å of bound ADP. These are Ala^{38} (human Ser^{52}) and Leu^{173} (human Val^{186}), which are ~4 and 5Å from the exocyclic N6 of the adenyl ring of ADP, respectively. Consequently, all the key interactions with ADP, ATP, and various HSP90 inhibitors are essentially the same. Comparison of the binding of CCT018159 with the yeast and human HSP90α confirms a high degree of similarity (36).

Dissociation constants (K_d values) determined by isothermal titration calorimetry were similar for CCT018159 and 17-AAG but higher than for radicicol. The human HSP90 ATPase-activating protein AHA1 did not appreciably alter the CCT018159 K_d and had no effect on enzyme inhibition. Compared with CCT018159, analogues CCT072440 and CCT072453 (Fig. 1) showed improved binding to, and inhibition of, both yeast protein and human full-length HSP90, as measured by a variety of assays. Structure-activity relationships for a larger analogue series supports the importance of the interaction of 5′-substituents, especially ethyl and chloro, with the hydrophobic pocket mentioned above (35–37). Replacement of 5′-ethyl in CCT018159 with 5′-chloro in both CCT072440 and CCT072453 improves potency, whereas CCT066961, lacking the 5′-substituent, is much less potent in all biological assays.

Enzyme kinetic analysis showed that CCT018159, 17-AAG, and geldanamycin inhibit human HSP90 competitively with respect to ATP, consistent with the binding mode, and have similar K_i values.

Concerning biochemical selectivity, CCT018159 was inactive against two other ATPases (i.e., the structurally related human topoisomerase II and the structurally unrelated but biologically linked HSP72). In addition, CCT018159 exhibited generally weak activity at 50 μmol/L against various kinases, with the exception of LCK. Thus, CCT018159 exhibits promising selectivity for a lead compound against HSP90. It is likely that selectivity will be improved even further during lead optimization.

In terms of antiproliferative properties against HCT116 human colon cancer cells, the modest 2- to 3-fold increase in enzyme potency compared with CCT018159 seen for the 5′-chloro compounds was not translated into cellular activity, presumably due to physicochemical and permeability factors. More significantly, although the pyrazole compounds have similar micromolar potency against HSP90β to 17-AAG, the latter is more potent in cells; however, in some tumor lines, the difference was only 3- to 10-fold. This discrepancy between target and cell activity is not surprising for 17-AAG; several groups have reported that 17-AAG possesses moderate micromolar target potency while achieving low nanomolar growth inhibition in many but not all cell lines (15, 49). Chiosis et al. suggested that the differential cell versus target potency for 17-AAG may be explained by the physicochemical characteristics of ansamycins, leading to high intracellular concentrations (49). Kamal et al. (5) reported that 17-AAG binds to HSP90 more tightly in the presence of certain co-chaperones, and that a high-affinity, 17-AAG–sensitive superchaperone complex predominates in cancer cells compared with normal epithelial and endothelial cells. This could explain the greater accumulation in tumor tissue and the reported preferential activity of 17-AAG towards malignant versus normal cells (49). Interestingly, although

we found that CCT018159 and 17-AAG were bound about 2-fold more tightly to HSP90 in cell lysates compared with recombinant HSP90β, we observed with both CCT018159 and 17-AAG that binding to HSP90 was comparable in lysates from cancer and nontumorigenic cells. Similar results were reported by others (27, 50, 51). One explanation for these apparent discrepancies between different studies is that geldanamycin exhibits slow tight binding inhibition, potentially related to conversion of the quinone to the more potent hydroquinone (25, 27, 50, 51). This is consistent with our original observation that 17-AAG is much more potent in cancer cells overexpressing the quinone reductase NQO1, which we showed reduces 17-AAG (15, 25). We did not observe a time-dependent increase in HSP90β binding potency with 17-AAG. The disparities between various studies could relate to the different binding probes and experimental conditions, especially the presence of reducing agents. Here, we used a fluorescent CCT018159 derivative as the binding probe and did not include reducing agents. Of note, Gooljarsingh et al. (50) observed a time-dependent increase in binding with 17-AAG, but not with an isoxazole analogue related to CCT018159, in agreement with our results. It seems possible that, lacking the quinone moiety of the geldanamycins, the biochemical and cellular pharmacology of the pyrazole resorcinols may be less complex.

In contrast to 17-AAG, the lack of dependence of the pyrazole resorcinols on NQO1 was expected as the pyrazoles have no quinone. NQO1 expression varies across tumor and healthy tissues, and NQO1 polymorphism is associated with loss of activity (52). Thus, the independence of the pyrazole resorcinols from NQO1 activity removes a source of metabolic variability and a potential resistance mechanism. Quinone metabolism may contribute to ansaymcin liver toxicity, and it will be interesting to assess the toxicology of the new series using analogues with optimized pharmacokinetic properties.

As with NQO1, the cellular activities of CCT018159 and its analogues are also independent of P-glycoprotein expression. In addition, both the pyrazole resorcinols and 17-AAG are able to retain activity in cancer cells with acquired resistance to oxaliplatin where the resistance was associated with reduced platinum-DNA adduct formation (45). Our results do, however, suggest that care should be taken in considering the potential for resistance to CCT018159 and related compounds through metabolism of the resorcinol moiety to glucuronides. Crystal structures (Fig. 2) show that these metabolites could not bind HSP90. Uridine diphospho-glucuronosyltransferases, which catalyze glucuronidation of phenolic hydroxyls, are known to be variably expressed in certain colon, liver, and kidney cancers (53).

Given previous results with 17-AAG (5), it is of interest to compare the activity of CCT018159 in cancer versus nonmalignant cells. Interestingly, HUVECs were particularly sensitive to the growth inhibition by CCT018159 compared with tumor cells. However, two other nontumorigenic epithelial cell lines (MCF10a mammary and PNT2 prostate) showed in general similar or rather reduced sensitivity sensitive to CCT018159 compared with most of the tumor lines. With 17-AAG, HUVEC sensitivity approached that of the most sensitive cancer cells, whereas the nontumorigenic breast and prostate lines tended to have GI_{50} values closer to those of the more resistant cancer lines.

Clinical studies with 17-AAG showed that doses that were quite well tolerated, apart from issues with the DMSO-containing formulation, gave good pharmacokinetic exposures resulting in HSP90 inhibition in tumor biopsies, as shown by the validated molecular signature of HSP72 up-regulation and down-regulation of C-RAF and CDK4 proteins (17–20). Prolonged stable disease was seen in two melanoma patients (17). Melanoma cells are commonly driven by and addicted to the RAS-RAF-mitogen-activated protein/ERK kinase (MEK)-ERK pathway (54). In melanomas, where this pathway is activated by N-RAS mutation resulting in C-RAF activation, C-RAF depletion by CCT018159 or 17-AAG results in reduced ERK1/2 phosphorylation. Mutations in B-RAF, particularly the V600E form, are common in melanoma (55). We and others showed that B-RAF is a hypersensitive HSP90 client compared with wild type, and that 17-AAG stimulates B-RAF degradation (6, 7). Two of the melanoma cell lines used here (SKMEL 2 and SKMEL 5) have wild-type B-RAF, and SKMEL 28 and WM266.4 cells harbored mutant B-RAF (V600E and V600D, respectively; ref. 46). Both CCT018159 and 17-AAG reduced B-RAF protein expression, with the mutants being more sensitive in each case. As reported for 17-AAG (6, 7), CCT018159 sensitivity did not correlate with B-RAF status in the melanoma cells. Down-regulation of ERK1/2 activation is achieved by HSP90 inhibitors depleting either or both the C-RAF and mutant B-RAF drivers of the pathway. Thus, their therapeutic activity may be broader than MEK inhibitors, which show selective activity in B-RAF mutant melanomas (54).

Both CCT018159 and 17-AAG caused accumulation of melanoma and other tumor cells in G_1, as seen for 17-AAG in several but not all tumor lines (11, 16). The stage of cell cycle block by HSP90 inhibitors is cell line and tumor type dependent; for example, G_2-M arrest is seen in some colon cancer cell lines (11, 16). With the melanoma lines, G_1 arrest by both CCT018159 and 17-AAG is consistent with a predominant effect on the critical RAS-RAF-MEK-ERK1/2 pathway that regulates cyclin D1 expression in this tumor type (54). In addition to the same cell cycle effects, we show here that CCT018159 and 17-AAG both induced apoptosis in melanoma cells at equivalent growth inhibitory concentrations ($5 \times GI_{50}$). The results suggested a greater degree of detached apoptotic cells for CCT08159 than for 17-AAG at 24 h. At 48 h, more apoptotic cells were present with 17-AAG, whereas a greater amount of cell debris was seen with CCT018159. Further studies are required in melanoma and other cell lines to determine any consistent or cell line–specific effects that may be seen in the concentration- and time-dependent effects of the two agents. However, it is clear that both CCT018159 and 17-AAG induce cell cycle arrest and apoptosis.

CCT018159 modulates expression of several key proteins in HUVEC, including HSP72, AKT, and VEGFR-2, confirming that it inhibits HSP90 activity in these cells at concentrations used in functional assays. CCT018159 inhibited HUVEC chemotactic responses to soluble ligands, as well as haptotactic motility, which was associated with decreased FAK phosphorylation. Haptotaxis and tubular differentiation on Matrigel were also inhibited in two different types of human tumor cells. Thus, in addition to inhibiting cell cycle progression and inducing apoptosis, the diaryl pyrazole resorcinol HSP90 inhibitors are likely, as with 17-AAG (38), to exert antiangiogenic and anti-invasive effects *in vivo*. We also showed recently that CCT018159 and 17-AAG induce keratinocyte differentiation (56). Their combinatorial effects on the multiple phenotypic features of malignancy is a major advantage of HSP90 inhibitors. It is promising that this is shared by the geldanamycin, purine, and diaryl pyrazole series (8, 30).

Our objective here was to use CCT018159 and its analogues to exemplify the detailed biological properties of our new diaryl pyrazole resorcinol series of HSP90 inhibitors. The results show that CCT018159 represents the prototype of a novel, synthetic HSP90 inhibitor chemotype with potential advantages over 17-AAG in

terms of aqueous solubility, lack of susceptibility to P-glycoprotein, and independence from metabolism by NQO1. Absence of the quinone moiety may reduce hepatotoxicity. The resorcinol hydroxyls are, however, subject to glucuronidation. We recently showed that CCT018159 and its analogues have promising pharmacokinetic properties in mice (44). Structure-based lead optimization has produced more active inhibitors with similar cellular potency to 17-AAG and considerable potential to become a clinical candidate (36). Combinatorial action of HSP90 inhibitors against multiple oncogenic proteins and pathways, which provide the opportunity to modulate all the hallmarks of traits of cancer (8), is a significant feature of these agents. Given the considerable interest in HSP90 as an oncology drug target and the potential limitations of 17-AAG, it seems appropriate to progress several chemical series into preclinical and clinical development. Studies to date with other classes of HSP90 inhibitors have clearly indicated their ability to exhibit therapeutic selectivity for cancer versus normal tissues in animal models (15, 57). Assessment of therapeutic index will need to be carried out with more fully optimized diaryl pyrazole resorcinol analogues, including determination of effects on those organs for which toxicity has been reported for HSP90 inhibitors, including liver and heart, together with rapidly proliferating tissues, such as gastrointestinal tract and bone marrow.

Acknowledgments

Received 9/19/2006; revised 11/30/2006; accepted 12/28/2006.

Grant support: Cancer Research UK [CUK] programme grant C309/A2187 and Wellcome Trust. Paul Workman is a Cancer Research UK Life Fellow. Alison Maloney, Marissa Powers and Sharon Sanderson are recipients of PhD studentships from The Institute of Cancer Research.

The costs of publication of this article were defrayed in part by the payment of page charges. This article must therefore be hereby marked *advertisement* in accordance with 18 U.S.C. Section 1734 solely to indicate this fact.

We thank many colleagues and collaborators for helpful discussion, especially in the Chaperone Project Team and Signal Transduction and Molecular Pharmacology Team at The Institute of Cancer Research and also at Vernalis Ltd.; Jenny Titley for flow cytometry; and Amin Mirza, Bernard Nutley, and Andrew Dick for structural spectroscopic studies.

References

1. Maloney A, Workman P. HSP90 as a new therapeutic target for cancer therapy: the story unfolds. Expert Opin Biol Ther 2002;2:3–24.

2. Panaretou B, Prodromou C, Roe SM, et al. ATP binding and hydrolysis are essential to the function of the Hsp90 molecular chaperone *in vivo*. EMBO J 1998;17:4829–36.

3. Connell P, Ballinger CA, Jiang J, et al. The co-chaperone CHIP regulates protein triage decisions mediated by heat-shock proteins. Nat Cell Biol 2001;3:93–6.

4. Pearl LH, Prodromou C. Structure and mechanism of the hsp90 molecular chaperone machinery. Annu Rev Biochem 2006;75:271–94.

5. Kamal A, Thao L, Sensintaffar J, et al. A high-affinity conformation of Hsp90 confers tumour selectivity on Hsp90 inhibitors. Nature 2003;425:407–10.

6. da Rocha DS, Friedlos F, Light Y, Springer C, Workman P, Marais R. Activated B-RAF is an Hsp90 client protein that is targeted by the anticancer drug 17-allylamino-17-demethoxygeldanamycin. Cancer Res 2005;65:10686–91.

7. Grbovic OM, Basso AD, Sawai A, et al. V600E B-Raf requires the Hsp90 chaperone for stability and is degraded in response to Hsp90 inhibitors. Proc Natl Acad Sci U S A 2006;103:57–62.

8. Workman P. Combinatorial attack on multistep oncogenesis by inhibiting the Hsp90 molecular chaperone. Cancer Lett 2004;206:149–57.

9. Roe SM, Prodromou C, O'Brien R, Ladbury JE, Piper PW, Pearl LH. Structural basis for inhibition of the Hsp90 molecular chaperone by the antitumor antibiotics radicicol and geldanamycin. J Med Chem 1999;42:260–6.

10. Schulte TW, An WG, Neckers LM. Geldanamycin-induced destabilization of Raf-1 involves the proteasome. Biochem Biophys Res Commun 1997;239:655–9.

11. Munster PN, Basso A, Solit D, Norton L, Rosen N. Modulation of Hsp90 function by ansamycins sensitizes breast cancer cells to chemotherapy-induced apoptosis in an RB- and schedule-dependent manner. See: E.A. Sausville, Combining cytotoxics and 17-allylamino, 17-demethoxygeldanamycin: sequence and tumor biology matters. Clin Cancer Res 2001;7:2228–36, 2155–8.

12. Whitesell L, Shifrin SD, Schwab G, Neckers LM. Benzoquinonoid ansamycins possess selective tumoricidal activity unrelated to src kinase inhibition. Cancer Res 1992;52:1721–8.

13. Supko JG, Hickman RL, Grever MR, Malspeis L. Preclinical pharmacologic evaluation of geldanamycin as an antitumor agent. Cancer Chemother Pharmacol 1995;36:305–15.

14. Schulte TW, Neckers LM. The benzoquinone ansamycin 17-allylamino-17-demethoxygeldanamycin binds to HSP90 and shares important biologic activities with geldanamycin. Cancer Chemother Pharmacol 1998;42:273–9.

15. Kelland LR, Sharp SY, Rogers PM, Myers TG, Workman P. DT-Diaphorase expression and tumor cell sensitivity to 17-allylamino, 17-demethoxygeldanamycin, an inhibitor of heat shock protein 90. J Natl Cancer Inst 1999;91:1940–9.

16. Hostein I, Robertson D, DiStefano F, Workman P, Clarke PA. Inhibition of signal transduction by the Hsp90 inhibitor 17-allylamino-17-demethoxygeldanamycin results in cytostasis and apoptosis. Cancer Res 2001;61:4003–9.

17. Banerji U, O'Donnell A, Scurr M, et al. Phase I pharmacokinetic and pharmacodynamic study of 17-allylamino, 17-demethoxygeldanamycin in patients with advanced malignancies. J Clin Oncol 2005;23:4152–61.

18. Goetz MP, Toft D, Reid J, et al. Phase I trial of 17-allylamino-17-demethoxygeldanamycin in patients with advanced cancer. J Clin Oncol 2005;23:1078–87.

19. Pacey S, Banerji U, Judson I, Workman P. Hsp90 inhibitors in the clinic. Handb Exp Pharmacol 2006;172:331–58.

20. Banerji U, Walton M, Raynaud F, et al. Pharmacokinetic-pharmacodynamic relationships for the heat shock protein 90 molecular chaperone inhibitor 17-allylamino, 17-demethoxygeldanamycin in human ovarian cancer xenograft models. Clin Cancer Res 2005;11:7023–32.

21. Modi S, Stopeck A, Gordon MS, et al. Phase I trial of KOS-953, a heat shock 90 inhibitor, and trastuzumab (T). J Clin Oncol 2006;24:3s.

22. Chanan-Khan A, Richardson P, Alsina M, et al. Phase I clinical trial of KOS-953 + bortezomib (BZ) in relapsed refractory multiple myeloma (MM). J Clin Oncol 2006;24:137.

23. Egorin MJ, Zuhowski EG, Rosen DM, Sentz DL, Covey JM, Eiseman JL. Plasma pharmacokinetics and tissue distribution of 17-(allylamino)-17-demethoxygeldanamycin (NSC 330507) in CD2F1 mice. Cancer Chemother Pharmacol 2001;47:291–302.

24. Egorin MJ, Rosen DM, Wolff JH, Callery PS, Musser SM, Eiseman JL. Metabolism of 17-(allylamino)-17-demethoxygeldanamycin (NSC 330507) by murine and human hepatic preparations. Cancer Res 1998;58:2385–96.

25. Guo W, Reigan P, Siegel D, Zirrolli J, Gustafson D, Ross D. Formation of 17-allylamino-demethoxygeldanamycin (17-AAG) hydroquinone by NAD(P)H:quinone oxidoreductase 1: role of 17-AAG hydroquinone in heat shock protein 90 inhibition. Cancer Res 2005;65:10006–15.

26. Kaur G, Belotti D, Burger AM, et al. Antiangiogenic properties of 17-(dimethylaminoethylamino)-17-demethoxygeldanamycin: an orally bioavailable heat shock protein 90 modulator. Clin Cancer Res 2004;10:4813–21.

27. Ge J, Normant E, Porter JR, et al. Design, synthesis, and biological evaluation of hydroquinone derivatives of 17-amino-17-demethoxygeldanamycin as potent, water-soluble inhibitors of Hsp90. J Med Chem 2006;49:4606–15.

28. Soga S, Shiotsu Y, Akinaga S, Sharma SV. Development of radicicol analogues. Curr Cancer Drug Targets 2003;3:359–69.

29. McDonald E, Workman P, Jones K. Inhibitors of the HSP90 molecular chaperone: attacking the master regulator in cancer. Curr Top Med Chem 2006;6:1091–107.

30. Chiosis G, Rodina A, Moulick K. Emerging Hsp90 inhibitors: from discovery to clinic. Anticancer Agents Med Chem 2006;6:1–8.

31. Sharp S, Workman P. Inhibitors of the HSP90 molecular chaperone: current status. Adv Cancer Res 2006;95:323–48.

32. Chiosis G, Timaul MN, Lucas B, et al. A small molecule designed to bind to the adenine nucleotide pocket of Hsp90 causes Her2 degradation and the growth arrest and differentiation of breast cancer cells. Chem Biol 2001;8:289–99.

33. Chiosis G. Discovery and development of purine-scaffold hsp90 inhibitors. Curr Top Med Chem 2006;6:1183.

34. Rowlands MG, Newbatt YM, Prodromou C, Pearl LH, Workman P, Aherne W. High-throughput screening assay for inhibitors of heat-shock protein 90 ATPase activity. Anal Biochem 2004;327:176–83.

35. Cheung KM, Matthews TP, James K, et al. The identification, synthesis, protein crystal structure and *in vitro* biochemical evaluation of a new 3,4-diarylpyrazole class of Hsp90 inhibitors. Bioorg Med Chem Lett 2005;15:3338–43.

36. Dymock BW, Barril X, Brough PA, et al. Novel, potent small-molecule inhibitors of the molecular chaperone Hsp90 discovered through structure-based design. J Med Chem 2005;48:4212–5.

37. McDonald E, Jones K, Brough PA, Drysdale MJ, Workman P. Discovery and development of pyrazole-scaffold Hsp90 inhibitors. Curr Top Med Chem 2006;6:1193–203.

38. Sanderson S, Valenti M, Gowan S, et al. Benzoquinone ansamycin heat shock protein 90 inhibitors modulate multiple functions required for tumor angiogenesis. Mol Cancer Ther 2006;5:522–32.

39. Prodromou C, Piper PW, Pearl LH. Expression and crystallization of the yeast Hsp82 chaperone, and preliminary X-ray diffraction studies of the amino-terminal domain. Proteins 1996;25:517–22.

40. Panaretou B, Siligardi G, Meyer P, et al. Activation of

the ATPase activity of hsp90 by the stress-regulated cochaperone aha1. Mol Cell 2002;10:1307–18.
41. Howes R, Barril X, Dymock BW, et al. A fluorescence polarization assay for inhibitors of Hsp90. Anal Biochem 2006;350:202–13.
42. Hardcastle A, Boxall K, Richards J, et al. Solid-phase immunoassays in mechanism-based drug discovery: their application in the development of inhibitors of the molecular chaperone heat-shock protein 90. Assay Drug Dev Technol 2005;3:273–85.
43. Jones NP, Peak J, Brader S, Eccles SA, Katan M. PLCgamma1 is essential for early events in integrin signalling required for cell motility. J Cell Sci 2005;118: 2695–706.
44. Smith NF, Hayes A, James K, et al. Preclinical pharmacokinetics and metabolism of a novel diaryl pyrazole resorcinol series of heat shock protein 90 inhibitors. Mol Cancer Ther 2006;5:1628–37.
45. Sharp SY, O'Neill CF, Rogers P, Boxall FE, Kelland LR. Retention of activity by the new generation platinum agent AMD0473 in four human tumour cell lines possessing acquired resistance to oxaliplatin. Eur J Cancer 2002;38:2309–15.
46. Davies H, Bignell GR, Cox C, et al. Mutations of the BRAF gene in human cancer. Nature 2002;417:949–54.
47. Calalb MB, Polte TR, Hanks SK. Tyrosine phosphorylation of focal adhesion kinase at sites in the catalytic domain regulates kinase activity: a role for Src family kinases. Mol Cell Biol 1995;15:954–63.
48. Kreusch A, Han S, Brinker A, et al. Crystal structures of human HSP90alpha-complexed with dihydroxyphenylpyrazoles. Bioorg Med Chem Lett 2005;15:1475–8.
49. Chiosis G, Huezo H, Rosen N, Mimnaugh E, Whitesell L, Neckers L. 17AAG: low target binding affinity and potent cell activity-finding an explanation. Mol Cancer Ther 2003;2:123–9.
50. Gooljarsingh LT, Fernandes C, Yan K, et al. A biochemical rationale for the anticancer effects of Hsp90 inhibitors: Slow, tight binding inhibition by geldanamycin and its analogues. Proc Natl Acad Sci U S A 2006;103:7625–30.
51. Maroney AC, Marugan JJ, Mezzasalma TM, et al. Dihydroquinone ansamycins: toward resolving the conflict between low *in vitro* affinity and high cellular potency of geldanamycin derivatives. Biochemistry 2006; 45:5678–85.
52. Traver RD, Siegel D, Beall HD, et al. Characterization of a polymorphism in NAD(P)H: quinone oxidoreductase (DT-diaphorase). Br J Cancer 1997;75:69–75.
53. Nagar S, Remmel RP. Uridine diphosphoglucuronosyltransferase pharmacogenetics and cancer. Oncogene 2006;25:1659–72.
54. Solit DB, Garraway LA, Pratilas CA, et al. BRAF mutation predicts sensitivity to MEK inhibition. Nature 2006;439:358–62.
55. Wellbrock C, Ogilvie L, Hedley D, et al. V599EB-RAF is an oncogene in melanocytes. Cancer Res 2004;64:2338–42.
56. Honma M, Stubbs M, Collins I, Workman P, Aherne W, Watt FM. Identification of novel keratinocyte differentiation modulating compounds by high-throughput screening. J Biomol Screen 2006;11:1–8.
57. Chiosis G, Lucas B, Huezo H, Solit D, Basso A, Rosen N. Development of purine-scaffold small molecule inhibitors of Hsp90. Curr Cancer Drug Targets 2003;3: 371–6.
58. Sharp SY, Kelland LR, Valenti MR, Brunton LA, Hobbs S, Workman P. Establishment of an isogenic human colon tumor model for NQO1 gene expression: application to investigate the role of DT-diaphorase in bioreductive drug activation *in vitro* and *in vivo*. Mol Pharmacol 2000;58:1146–55.
59. Sharp SY, Rowlands MG, Jarman M, Kelland LR. Effects of a new antioestrogen, idoxifene, on cisplatin- and doxorubicin-sensitive and -resistant human ovarian carcinoma cell lines. Br J Cancer 1994;70:409–14.